LARGE EDDY SIMULATIONS OF THE TURBULENT FLOW BETWEEN A ROTATING AND A STATIONARY DISK

Magne Lygren and Helge I. Andersson
Division of Applied Mechanics
Norwegian University of Science and Technology
N-7491 Trondheim, NORWAY
helge.i.andersson@maskin.ntnu.no

ABSTRACT

Large eddy simulations of the flow between a rotating and a stationary disk have been performed using a dynamic and a mixed dynamic subgrid-scale model. The simulations were compared to direct numerical simulation results. The mixed dynamic model gave better overall predictions than the dynamic model. Modifications of the mean flow three-dimensionality on the near-wall structures were also investigated. Conditional averages near strong stress-producing events led to the same conclusions regarding these modifications as studies of the flow generated by direct numerical simulation.

INTRODUCTION

A three-dimensional turbulent boundary layer (3DTBL) is a wall-bounded flow where the direction of the mean velocity varies with the distance from the wall. Although the turbulence statistics and structure are similar for 3D and 2D boundary layers, there are some well-known differences: The vector formed by the turbulence stress is not aligned with the mean strain rate in a 3DTBL, and the turbulence stress/intensity ratio is reduced in 3DTBLs as compared to 2D boundary layers; see e.g. Durbin (1993), Eaton (1995) and Johnston & Flack (1996).

In most 3DTBLs studied, the cause of the three-dimensionality is a sudden spatial or temporal change in the flow conditions. In contrast, the flow between a rotating and a stationary disk is three-dimensional from the inception. Together with the flow over one rotating disk (Littell & Eaton, 1994), the turbulent Ekman layer (Coleman *et al.*, 1990) and the 3DTBL created by a rotating free-stream velocity vector (Spalart, 1989), the rotor-stator flow is therefore well suited to study effects of the mean-flow three-dimensionality on the turbulence without strong effects from system parameters such as streamwise pressure gradients, geometry and initial conditions.

While direct numerical simulations (DNS) are applicable to low-Reynolds number flows, all scales in the turbulence can not be resolved in flows at higher Reynolds numbers. In large eddy simulations (LES) the smallest scales in the turbulence are modeled by a subgrid-scale (SGS) model, while the large energy-containing eddies are resolved directly. In the classical SGS model by Smagorinsky (1963) a model parameter has to be specified *a priori*. In the dynamical model by Germano *et al.* (1991) and the mixed dynamical model by Vreman *et al.* (1994) this parameter is calculated from the resolved flow field.

The main objective of this work is to apply LES together with the dynamic and the mixed dynamic SGS models to predict the flow in the gap between a rotating and a stationary disk. The simulations are evaluated by comparing with the DNS results of the same flow configuration by Lygren & Andersson (2001). Additionally the applicability of LESs to study the underlying near-wall coherent structures is examined.

PROBLEM FORMULATION

In large eddy simulations the filtered incompressible Navier-Stokes equations are studied:

$$\frac{\partial \overline{u}_j}{\partial x_j} = 0 \tag{1}$$

$$\frac{\partial \overline{u}_i}{\partial t} + \frac{\partial \overline{u}_i \overline{u}_j}{\partial x_j} = -\frac{\partial \overline{p}}{\partial x_i} + \frac{\partial}{\partial x_j}\left(2\nu \overline{S}_{ij} - \tau_{ij}\right) \tag{2}$$

An overbar denotes variables filtered on grid level. $\tau_{ij} = \overline{u_i u_j} - \overline{u}_i \overline{u}_j$ are the subgrid-scale stresses which are introduced from the filtering of the non-linear term in the momentum equation, and $\overline{S}_{ij} = (\partial \overline{u}_i / \partial x_j + \partial \overline{u}_j / \partial x_i)/2$.

In the dynamic model by Germano *et al.* (1991) the Smagorinsky eddy-viscosity is used in expressing τ_{ij}:

$$\tau_{ij} - \frac{\delta_{ij}}{3}\tau_{kk} = -2\nu_T \overline{S}_{ij} \qquad (3)$$

The eddy viscosity ν_T is defined as

$$\nu_T = C_s^2 \Delta^2 |\overline{S}|, \qquad (4)$$

where $|\overline{S}| = (2\overline{S}_{ij}\overline{S}_{ij})^{1/2}$, C_s is the Smagorinsky coefficient and Δ is a length-scale of the filter width. In the dynamic approach C_s^2 is evaluated by introducing a wider test filter $\widehat{\cdot}$ of length-scale $\widehat{\Delta}$. Assuming that C_s^2 is equal on the grid-filter-level and the test-filter-level, the Smagorinsky coefficient is expressed as

$$C_s^2(x_i,t) = -\frac{1}{2}\frac{\langle L_{ij} M_{ij} \rangle}{\langle M_{ij} M_{ij} \rangle}, \qquad (5)$$

where $L_{ij} = \widehat{\overline{u_i}\overline{u_j}} - \widehat{\overline{u}}_i \widehat{\overline{u}}_j$ and $M_{ij} = \Delta^2 \left(\alpha^2 |\widehat{\overline{S}}| \widehat{\overline{S}}_{ij} - \widehat{|\overline{S}|\overline{S}_{ij}} \right)$. To avoid that the denominator in equation (5) becomes zero, the equation is usually averaged (indicated by $\langle\rangle$) in homogeneous directions. The only adjustable parameter is thus the ratio α between the length scales $\Delta/\widehat{\Delta}$.

In the mixed dynamic model by Vreman *et al.* (1994) a similarity model is used together with the Smagorinsky model to express the SGS stresses:

$$\tau_{ij} - \frac{\delta_{ij}}{3}\tau_{kk} = -2\nu_T \overline{S}_{ij} + \mathcal{L}_{ij}^m - \frac{\delta_{ij}}{3}\mathcal{L}_{kk}^m \qquad (6)$$

Here, the modified Leonard stresses $\mathcal{L}_{ij}^m = \overline{\overline{u_i}\overline{u_j}} - \overline{\overline{u}}_i \overline{\overline{u}}_j$ have been introduced. The Smagorinsky coefficient is in the mixed model evaluated as

$$C_s^2(x_i,t) = -\frac{1}{2}\frac{\langle (L_{ij} - H_{ij}) M_{ij} \rangle}{\langle M_{ij} M_{ij} \rangle}, \qquad (7)$$

where $H_{ij} = \widehat{\overline{\overline{u}}_i \overline{\overline{u}}_j} - \widehat{\overline{\overline{u}}}_i \widehat{\overline{\overline{u}}}_j - (\widehat{\overline{\overline{u_i}\overline{u_j}}} - \widehat{\overline{\overline{u}}_i \overline{\overline{u}}_j})$.

To achieve a feasible simulation of the flow between the disks, the computational domain consists of an angular section $\Delta\theta$ between the radial surfaces r_1 and r_2, see figure 1. In the tangential direction ordinary periodicity is used and no-slip is imposed at the two disks. In the radial direction ordinary periodicity is not applicable since statistical quantities vary with r. Wu & Squires (2000) applied quasi-periodic boundary conditions in the radial direction in a large eddy simulation of flow over a rotating disk. This approach was slightly modified

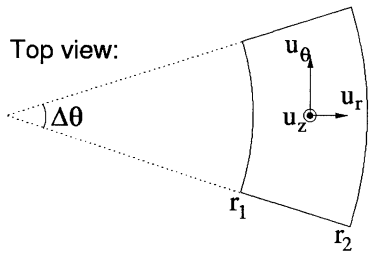

Figure 1: Sketch of the computational domain

by Lygren & Andersson (2001) in their DNS of rotor-stator flow. In the present study, this quasi-periodicity is adopted.

The governing equations (1) and (2) are discretized using second-order finite-differences in cylindrical coordinates. A second-order Adams-Bashforth scheme is used as time-advancement. The Poisson equation is solved by a fast multigrid method. The averaging $\langle\rangle$ in equations 5 and 7 is first performed in the tangential direction. Thereafter C_s^2 is expressed as $C_s^2(r,z,t) = C_0(z,t) + C_1(z,t)r$ where C_0 and C_1 are obtained in the least-squares sense from the tangential averages of $C_s^2(x_i,t)$.

The flow between infinite disks is locally characterized by the rotational Reynolds number $Re_r = r^2\omega/\nu$ and the local gap ratio $G = s/r$. Here r is the radial coordinate, ω the angular velocity of the rotating disk, ν the kinematic viscosity of the fluid and s the distance between the disks. The Reynolds number and gap ratio in the present study equal the parameters in the DNS by Lygren & Andersson (2001): $Re_{r_m} = 4 \cdot 10^5$ and $G_{r_m} = 0.02$ where $r_m = (r_1 + r_2)/2$. The size of the computational domain is $3.5s \times 14s \times s$ in the radial, tangential and axial directions. The corresponding number of grid points is $96 \times 48 \times 48$. In wall units the grid spacing is approximately 40×20 in the tangential and radial directions. The grid point closest to the disks is about 0.5 wall unit from the surface. The tangential length of the computational domain is twice the length of the domain used in the DNS in order to include more grid-points in the averages in equations (5) and (7).

RESULTS AND DISCUSSION

Turbulence statistics

Three LESs are performed on the same computational mesh using no SGS-model, the dynamic model of Germano *et al.* (1991) and the mixed dynamic model do to Vreman *et al.* (1994). The three mean velocity components are compared with DNS results of Lygren & Andersson (2001) in figure 2. The velocity components are averaged in tangential direc-

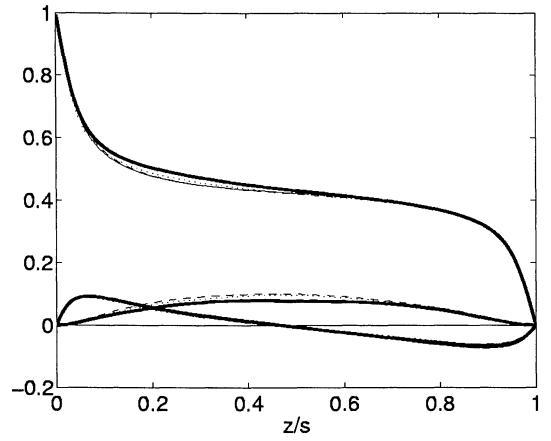

Figure 2: Mean velocities. The rotating disk is located at $z = 0$. Bold: DNS (Lygren & Andersson, 2001). ———, Vreman; – – –, Germano; ·····, no model.

	Re_τ Rotor	Re_τ Stator
DNS	265.7	213.5
No model	278.8	223.3
Germano	264.0	216.8
Vreman	267.7	214.3

Table 1: Reynolds numbers $Re_\tau = u_\tau s/\nu$, where $u_\tau = (\nu \partial U_\theta/\partial z)^{1/2}$, at the rotating and the stationary disk.

tion and in the radial direction after normalizing with the local disk speed ωr. The mean velocity components are relatively insensitive to the model used. The tangential mean velocity in the LES predictions is slightly underpredicted in the region $0.1 \leq z/s \leq 0.5$. This underprediction is actually smallest when no model is used.

The Reynolds numbers based on the friction velocity at the two disks are listed in table 1. When no model is used, the friction velocity is overpredicted by approximately 5% at both disks. In the simulation using Vreman's model, the results deviate less than 1% from the DNS.

Turbulence intensities and shear stresses are presented in figures 3 and 4. Tangential intensities are higher than the DNS data. The largest discrepancy is when no model is used and smallest for the Vreman model. The agreement is better near the stationary than at the rotating disk. The explanation is that the resolution in wall units is highest at the stationary disk.

The wall-normal intensities are underpredicted when the SGS models are used, in contrast to when no model is applied. This is a common feature of LESs using lower-order finite-differences, see e.g. Balaras *et al.* (1995), Kravchenko & Moin (1997) and Wu & Squires (2000).

The sum of the resolved and modeled turbulent shear stresses are presented in figure 4. $\overline{u_\theta u_z}$, which is the primary shear stress, is very well predicted by the simulation using the SGS model by Vreman. Germano's SGS model slightly underpredicts this stress, while the simulation without any model severely overpredicts it. The secondary shear stress, $\overline{u_r u_z}$, in figure 4b) is underpredicted in the central region in all the simulations, as compared to the DNS. The third shear stress, $\overline{u_\theta u_r}$, is generally of negligible importance in boundary layer calculations. The LESs fail to reproduce the significant negative dips near both disks, whereas $\overline{u_\theta u_r}$ is overpredicted in the core region. This third shear stress tend to converge statistically very slowly and further sampling would tend to smoothen the curves in figure 4c).

To gain further insight into the structure of the simulated turbulence, the anisotropy parameter $A = 1 - 9/8(A_2 - A_3)$ is shown in figure 5. A_2 and A_3 are the second and third invariants of the anisotropic part of the Reynolds stress:

$$A_2 = a_{ik}a_{ki} \text{ and } A_3 = a_{ik}a_{kl}a_{li},$$

where $a_{ij} = \overline{u_i' u_j'}/2k - \delta_{ij}/3$. A equals unity when the turbulence stress is isotropic and zero in two-component turbulence (Lumley, 1978). Figure 5 shows that A is relative insensitive to the SGS model used, and that A is reduced in the LESs as compared to the DNS. The reduced degree of isotropy is therefore an effect of the coarseness of the numerical grid. The underprediction of wall-normal fluctuations in the simulations using SGS model is therefore partially caused by the reduced level of $\overline{u_\theta u_\theta}$.

Turbulence structures

As shown in the previous section, the statistical predictions from the LESs are in reasonable good agreement with the DNS result by Lygren & Andersson (2001). Littell & Eaton (1994) showed that although there are strong similarities between 3DTBLs and 2DTBLs, the three-dimensionality of the mean flow slightly modifies the underlying turbulence structure. In 2DTBLs the main structures in the near-wall region are streamwise-oriented high- and low-speed streaks and quasi-streamwise vortices, see e.g. Robinson (1991) and Jeong *et al.* (1997). Lygren & Andersson (2000, 2001) examined the structures in the near-wall regions of the rotor-stator flow, and concluded that the quasi-streamwise vortices tend to produce weaker sweeps than the vortices found in 2DTBLs. Vortices of one sign of rotation were also responsible for generating most shear stress. This was found to be due

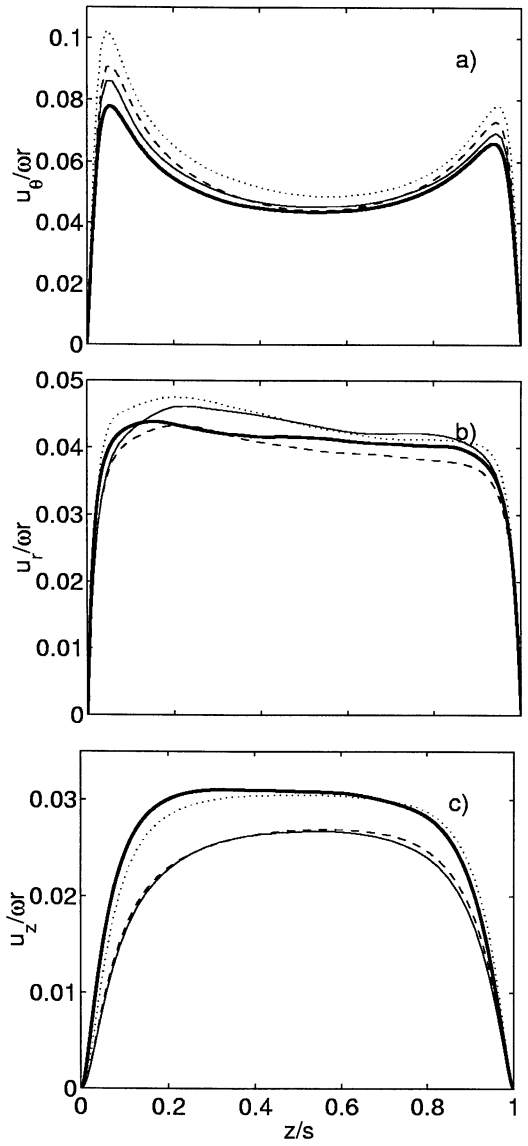

Figure 3: Turbulence intensities. Legends as in figure 2

both to an unequal number of vortices of each sign, and to the shear stress generated by individual vortices of one sign being stronger than the shear stress generated by oppositely rotating vortices.

The reliability of flow structures deduced from LESs is often questionable. It is therefore of interest to verify whether the modifications of the coherent structures by the three-dimensionality agree with the findings from the DNS by Lygren & Andersson (2001). Littell & Eaton (1994) analyzed the flow field near strong sweeps and ejections and observed a distinct asymmetry in the radial direction. This asymmetry is not possible in a 2DTBL. Kang *et al.* (1998) refined this study by performing a quadrant analysis of the field near the detection points. Lygren & Andersson (2000, 2001) also used a quadrant analysis technique in the study of the flow near strong ejections

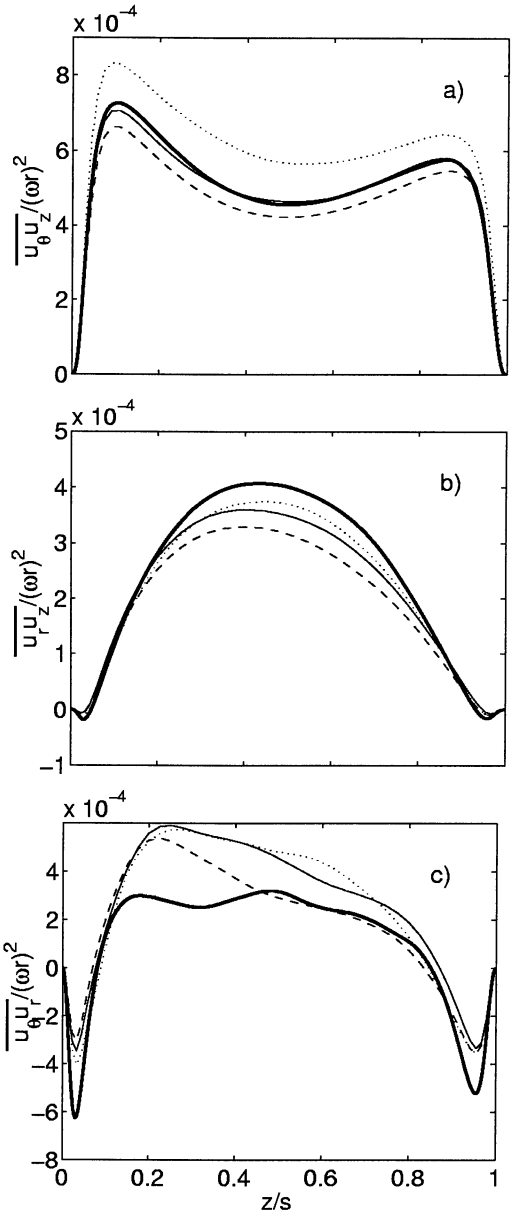

Figure 4: Turbulence shear stresses. In the simulations using Germano's and Vreman's SGS models the sum of the resolved and modeled stresses is shown. Legends as in figure 2

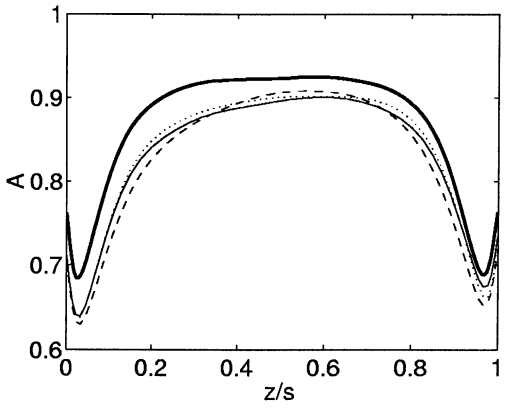

Figure 5: The parameter $A = 1 - 9/8(A_2 - A_3)$. Legends as in figure 2

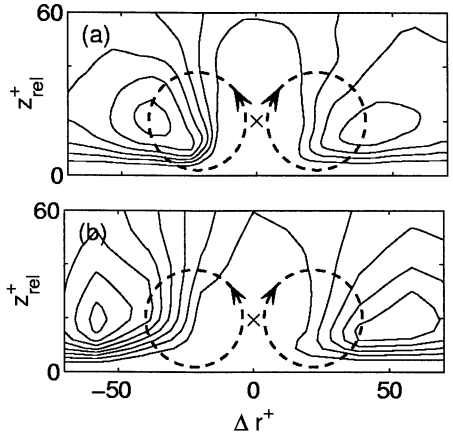

Figure 6: Contours of quadrant 4 contributions to $\overline{u_\theta u_z}$ near strong ejections. Near the rotating disk. a) DNS, Lygren & Andersson (2001). b) LES.

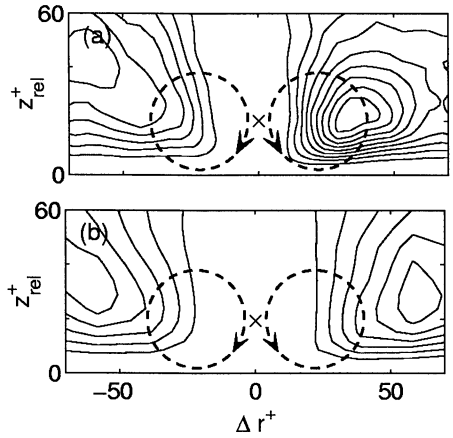

Figure 7: Contours of quadrant 2 contributions to $\overline{u_\theta u_z}$ near strong sweeps. Near the rotating disk. a) DNS, Lygren & Andersson (2001). b) LES.

and sweeps in the DNS of the rotor-stator flow. This analysis is here repeated of the flow field generated by the LES using Vreman's mixed SGS model.

In figure 6 isocontours of quadrant 4 (sweeps) contributions to the $\overline{u_\theta u_z}$-stress near strong quadrant 2 events (ejections) are shown. A strong ejection is defined as $u'_\theta u'_z > 3u'_{\theta,rms}u'_{z,rms}$ and $u_z > 0$. The position of the strong ejection is marked by a cross located at $\Delta r^+ = 0$ and $z^+_{rel} = 20$ where z_{rel} is the distance to the nearest disk. Since the quasi-streamwise vortices are associated with strong sweeps and ejections, the peaks on each side of the detection point are signatures of the two vortices generating the ejection. These vortices are indicated in figures 6 to 9. The quadrant 4 contribution is asymmetric relative to the origin $\Delta r^+ = 0$. This asymmetry, which is observed both in DNS (fig. 6a) and LES (fig. 6b), is not possible in 2DTBLs, and is therefore a consequence of the three-dimensionality

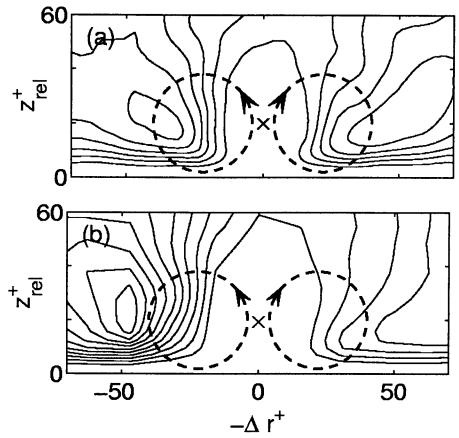

Figure 8: Contours of quadrant 4 contributions to $\overline{u_\theta u_z}$ near strong ejections. Near the stationary disk. a) DNS, Lygren & Andersson (2001). b) LES.

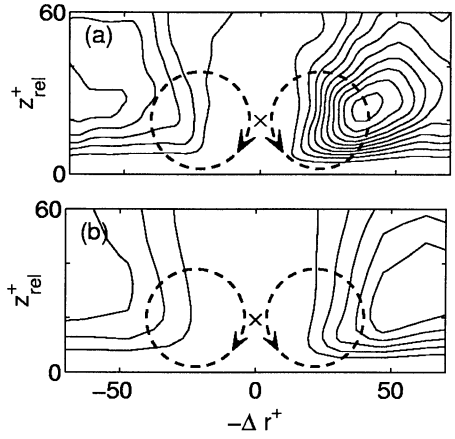

Figure 9: Contours of quadrant 2 contributions to $\overline{u_\theta u_z}$ near strong sweeps. Near the stationary disk. a) DNS, Lygren & Andersson (2001). b) LES.

of the mean flow. Since the peak is most pronounced for $\Delta r^+ < 0$, it is concluded that the left vortex is responsible for generating most of the strong ejections.

Figure 7 shows contours of quadrant 2 contributions to the $\overline{u_\theta u_z}$-stress near strong sweeps. A strong sweep is defined as $u_\theta u_z > 3u'_{\theta,rms}u'_{z,rms}$ and $u_z < 0$. As for the flow field near the strong ejections in figure 6, there are asymmetries between $\Delta r^+ < 0$ and $\Delta r^+ > 0$. The asymmetries in figure 7a) and 7b) are similar and the conditional averages from the DNS and LES therefore lead to the same conclusion, namely that the right vortex is responsible for generating most of the strong sweeps.

Likewise, the conditional averages near strong sweeps and ejections at the stator side in figures 8 and 9 closely resemble those obtained from the DNS, thus leading to the same conclusions as already drawn by Lygren & Andersson (2001).

SUMMARY

Large eddy simulations of the three-dimensional flow between a rotating and a stationary disk have been performed using finite-difference approximations. A dynamic and a mixed dynamic model were used to parameterize the SGS stresses. These simulations were compared with a LES without any SGS model and with recent DNS results. The main effect of the SGS models was to improve the predicted friction at the disks, and to improve the predictions of the streamwise turbulence intensity and the primary turbulence shear stress. The mixed dynamic model resulted in better predictions of the turbulence intensities and shear stresses than the dynamic model.

Near-wall structures in the flow field generated by the LES using the mixed dynamic model were analyzed with the view to study effects of the three-dimensionality of the mean flow. Conditional averaging was performed around strong ejections and sweeps. The conclusions to be drawn from this study confirm the conclusions already obtained from the DNS by Lygren & Andersson (2001). In spite of the moderate grid resolution used herein, the conditionally-averaged flow structures compare surprisingly well with those of the fully resolved DNS by Lygren & Andersson (2001). It is therefore conjectured that reliable information can be deduced also from conditionally-averaged flow structures in other LESs, provided that the grid resolution in wall units corresponds to that used in the present study.

References

BALARAS, E., BENOCCI, C. & PIOMELLI, U. 1995 Finite-difference computations of high Reynolds number flows using the dynamic subgrid-scale model. *Theoret. Comput. Fluid Dyn.* **7**, 207–216.

COLEMAN, G. N., FERZIGER, J. H. & SPALART, P. R. 1990 A numerical study of the turbulent Ekman layer. *J. Fluid Mech.* **213**, 313–348.

DURBIN, P. A. 1993 On modeling three-dimensional turbulent wall layers. *Phys. Fluids A* **5**, 1231–1238.

EATON, J. K. 1995 Effects of mean flow three dimensionality on turbulent boundary-layer structure. *AIAA Journal* **33**, 2020–2025.

GERMANO, M., PIOMELLI, U., MOIN, P. & CABOT, W. H. 1991 A dynamic subgrid-scale eddy viscosity model. *Phys. Fluids* **A 3**, 1760–1765.

JEONG, J., HUSSAIN, F., SCHOPPA, W. & KIM, J. 1997 Coherent structures near the wall in a turbulent channel flow. *J. Fluid Mech.* **332**, 185–214.

JOHNSTON, J. P. & FLACK, K. A. 1996 Review - advances in three dimensional turbulent boundary layers with emphasis on the wall-layer regions. *J. Fluids Engng.* **118**, 219–232.

KANG, H. S., CHOI, H. C. & YOO, J. Y. 1998 On the modification of the near-wall coherent structure in a three-dimensional turbulent boundary layer on a free rotating disk. *Phys. Fluids* **10**, 2315–2322.

KRAVCHENKO, A. & MOIN, P. 1997 On the effect of numerical errors in large eddy simulations of turbulent flows. *J. Comp. Phys.* **131**, 310–322.

LITTELL, H. S. & EATON, J. K. 1994 Turbulence characteristics of the boundary layer on a rotating disk. *J. Fluid Mech.* **266**, 175–207.

LUMLEY, J. L. 1978 Computational modeling of turbulent flows. *Adv. Appl. Mech.* **18**, 123–176.

LYGREN, M. & ANDERSSON, H. I. 2000 Near-wall structures in turbulent rotor-stator flow. In *Advances in Turbulence VIII*, pp. 675–678. CIMNE.

LYGREN, M. & ANDERSSON, H. I. 2001 Turbulent flow between a rotating and a stationary disk. *J. Fluid Mech.* **426**, 297–326.

ROBINSON, S. K. 1991 Coherent motions in the turbulent boundary layer. *Ann. Rev. Fluid Mech.* **23**, 601–639.

SMAGORINSKY, J. 1963 General circulation experiments with the primitive equations. i. the basic experiment. *Mon. Weather Rev.* **91**, 99–164.

SPALART, P. R. 1989 Theoretical and numerical study of a three-dimensional turbulent boundary layer. *J. Fluid Mech.* **205**, 319–340.

VREMAN, B., GEURTS, B. & KUERTEN, H. 1994 On the formulation of the dynamic mixed subgrid-scale model. *Phys. Fluids* **12**, 4057–4059.

WU, X. & SQUIRES, K. D. 2000 Prediction and investigation of the turbulent flow over a rotating disk. *J. Fluid Mech.* **418**, 231–264.